Second-line Sonazoid-enhanced ultrasonography for Liver Imaging Reporting and Data System category 3 and 4 on gadoxetate-enhanced magnetic resonance imaging

ULTRA SONO GRAPHY

ORIGINAL ARTICLE

https://doi.org/10.14366/usg.21198
pISSN: 2288-5919 • eISSN: 2288-5943
Ultrasonography 2022;41:519-529

Yeun-Yoon Kim[1]*, Ji Hye Min[1], Jeong Ah Hwang[1], Woo Kyoung Jeong[1], Dong Hyun Sinn[2], Hyo Keun Lim[1]

※Author affiliations appear at the end of this article.

Purpose: This study investigated the utility of second-line contrast-enhanced ultrasonography (CEUS) using Sonazoid in Liver Imaging Reporting and Data System category 3 (LR-3) and 4 (LR-4) observations on gadoxetate-enhanced magnetic resonance imaging (MRI).

Methods: This retrospective study included LR-3 or LR-4 observations on gadoxetate-enhanced MRI subsequently evaluated with CEUS from 2013 to 2017. The presence of MRI features, CEUS-arterial phase hyperenhancement (CEUS-APHE), and Kupffer phase defect (KPD) was evaluated. Multivariable logistic regression analysis was performed to identify significant imaging features associated with the diagnosis of hepatocellular carcinoma (HCC). The optimal diagnostic criteria were investigated using the McNemar test.

Results: In total, 104 patients with 104 observations (63 HCCs) were included. The presence of both CEUS-APHE and KPD on CEUS enabled the additional detection of 42.3% (11/26) of LR-3 HCCs and 78.4% (29/37) of LR-4 HCCs. Transitional phase (TP) hypointensity (adjusted odds ratio [OR], 10.59; P<0.001), restricted diffusion (adjusted OR, 7.55; P=0.004), and KPD (adjusted OR, 7.16; P=0.003) were significant imaging features for HCC diagnosis. The presence of at least two significant imaging features was optimal for HCC diagnosis (sensitivity, specificity, and accuracy: 88.9%, 78.1%, and 84.6%, respectively), with significantly higher sensitivity than the presence of both CEUS-APHE and KPD (sensitivity, specificity, and accuracy: 63.5% [P=0.001], 92.7% [P=0.077], and 75.0% [P=0.089], respectively).

Conclusion: The combined interpretation of gadoxetate-enhanced MRI and second-line CEUS using Sonazoid, focusing on TP hypointensity, restricted diffusion, and KPD, may be optimal for further characterizing LR-3 and LR-4 observations.

Keywords: Ultrasonography; Diagnosis; Carcinoma, Hepatocellular; Kupffer cells; Perfluorobutane

Key points: Transitional phase (TP) hypointensity, restricted diffusion, and Kupffer phase defect (KPD) were independently associated with hepatocellular carcinoma (HCC) diagnosis in Liver Imaging Reporting and Data System category 3 (LR-3) and category 4 (LR-4) observations. The presence of both contrast-enhanced ultrasonography (CEUS) arterial phase hyperenhancement and KPD on second-line CEUS could additionally detect 42.3% of LR-3 HCCs and 78.4% of LR-4 HCCs, and the enhancement pattern was only observed in HCCs in the LR-4 subgroup. Combined interpretation of magnetic resonance imaging and second-line CEUS using at least two significant imaging features (TP hypointensity, restricted diffusion, and KPD) was optimal for diagnosing HCC.

Received: September 18, 2021
Revised: January 23, 2022
Accepted: January 28, 2022

Correspondence to:
Ji Hye Min, MD, PhD, Department of Radiology and Center for Imaging Sciences, Samsung Medical Center, Sungkyunkwan University School of Medicine, 81 Irwon-ro, Gangnam-gu, Seoul 06351, Korea

Tel. +82-2-3410-0518
Fax. +82-2-3410-6368
E-mail: minjh1123@gmail.com

*Current affiliation: Department of Radiology and Research Institute of Radiological Science, Severance Hospital, Yonsei University College of Medicine, Seoul, Korea

How to cite this article:
Kim YY, Min JH, Hwang JA, Jeong WK, Sinn DH, Lim HK. Second-line Sonazoid-enhanced ultrasonography for Liver Imaging Reporting and Data System category 3 and 4 on gadoxetate-enhanced magnetic resonance imaging. Ultrasonography. 2022 Jul;41(3):519-529.

Introduction

The Liver Imaging Reporting and Data System (LI-RADS), with the latest computed tomography (CT)/magnetic resonance imaging (MRI) diagnostic algorithm released in 2018, has become one of the major diagnostic tools for hepatocellular carcinoma (HCC) in at-risk patients [1,2]. LI-RADS categories 3 (LR-3) and 4 (LR-4) are designated for hepatic observations that have an intermediate probability of HCC or are probably HCC. The pooled proportions of HCC were as high as 31% and 64% in LR-3 and LR-4 observations, respectively, according to a recent meta-analysis [3], but observations in each category were heterogeneous in terms of HCC probability [4]. The suggested management options for LR-3 and LR-4 observations range from repeated or alternative diagnostic imaging within 3 to 6 months to a multi-disciplinary discussion for a tailored workup [2,5]. Immediate second-line diagnostic tests may further stratify HCC probability in these observations, enabling timely treatment of HCC.

The use of contrast-enhanced ultrasonography (CEUS) with a perfluorobutane microbubble agent (Sonazoid) is strongly recommended to diagnose HCC in observations with atypical enhancement patterns on CT or gadoxetate-enhanced MRI according to the Asian Pacific Association for the Study of the Liver (APASL) guidelines [6]. CEUS using Sonazoid, which is not yet included in CEUS LI-RADS [7], has a unique property for functional imaging as the contrast agent is phagocytosed by Kupffer cells [8]. A defect in the Kupffer phase obtained 10 minutes after contrast injection suggests a lack of normal functioning Kupffer cells within the observation [9]. Therefore, the Kupffer phase is useful for characterizing hepatic nodules in the process of hepatocarcinogenesis; whereas a Kupffer phase defect (KPD) favors the diagnosis of progressed HCC, iso-enhancement in the Kupffer phase indicates earlier stages of hepatocarcinogenesis [10–13].

In LI-RADS, hepatobiliary phase (HBP) hypointensity on gadoxetate-enhanced MRI is regarded as an ancillary feature favoring malignancy in general [14]. On gadoxetate-enhanced MRI, the majority of high-grade dysplastic nodules and early HCCs are categorized as LR-3 or LR-4, mainly attributable to HBP hypointensity [15]. Meanwhile, a KPD identified using CEUS with Sonazoid appears in a more advanced stage of hepatocarcinogenesis than HBP hypointensity [10,12,16]. In addition, CEUS with Sonazoid may detect tumor vascularity with the help of real-time imaging and defect-reperfusion imaging [17,18]. For these reasons, the APASL guidelines recommend Sonazoid CEUS for characterizing observations without arterial phase hyperenhancement (APHE) but with HBP hypointensity on gadoxetate-enhanced MRI, which are likely to be categorized as LR-3 or LR-4 on LI-RADS [6].

LI-RADS restricts the timing of washout to the portal venous phase on gadoxetate-enhanced MRI, but this may limit the sensitivity for HCC diagnosis [19,20]. However, the APASL guidelines may be limited by low specificity for the diagnosis of HCC because they allow hypointensity in HBP as an alternative to washout after exclusion of cavernous hemangioma [21,22]. Therefore, the combined use of second-line CEUS features and gadoxetate-enhanced MRI features may help overcome these limitations of both guidelines, and maximize the unique advantages of both imaging modalities.

The purpose of this study was to investigate the utility of second-line CEUS using Sonazoid in the characterization of LR-3 and LR-4 observations on gadoxetate-enhanced MRI.

Materials and Methods

Compliance with Ethical Standards

The study protocol was in accordance with the ethical guidelines of the 1975 Declaration of Helsinki. The Institutional Review Board of Samsung Medical Center (approval number: 2019-08-026) approved this study and waived the requirement for patient consent as the study involved a retrospective review of medical records and images.

Patients

A review of medical records identified 543 potentially eligible patients with liver cirrhosis or chronic hepatitis B who underwent CEUS using Sonazoid for the evaluation of focal liver lesions from January 2013 to December 2017 at the authors' institution. The inclusion criteria were patients with (1) gadoxetate-enhanced MRI obtained within 3 months before CEUS, and (2) LR-3 or LR-4 observations <30 mm on gadoxetate-enhanced MRI based on LI-RADS version 2018. If there were multiple observations in a patient, the largest observation was selected for the analysis. The exclusion criteria were (1) patients with inadequate CEUS or MRI quality, (2) subsequent treatment of the index lesion with ablation therapy or radiotherapy, (3) loss to follow-up after CEUS, and (4) lack of a reference standard. The indications for CEUS at the authors' institution were (1) to characterize a lesion that was inconclusive on MRI, or (2) to increase the conspicuity of a lesion on ultrasonography to plan ablation therapy, upon request by referring physician.

There was a patient overlap with another study that compared the diagnostic performance of Sonazoid-enhanced CEUS and CT/MRI LI-RADS in LR-3, LR-4, LR-5, and LR-M lesions [23]. The present study investigated the added diagnostic value of Sonazoid-enhanced CEUS in LR-3 and LR-4 observations on MRI.

Image Acquisition

MRI scans were acquired using a 3.0-T system (Achieva, Philips Healthcare, Best, Netherlands). The routine protocol included dual-echo T1-weighted turbo field-echo images, breath-hold multi-shot T2-weighted images, respiratory-triggered single-shot heavily T2-weighted images, and respiratory-triggered single-shot echo-planar diffusion-weighted images with *b*-values of 0, 100, and 800 s/mm^2 (Supplementary Table 1). For dynamic contrast-enhanced imaging, T1-weighted three-dimensional turbo field-echo images were obtained before and after the intravenous administration of gadoxetate disodium (Primovist, Bayer Healthcare, Berlin, Germany) using a power injector at a rate of 1 mL/s for a total dose of 0.025 mmol/kg body weight, followed by a 20 mL saline flush. The arterial phase, portal venous phase, transitional phase (TP), and HBP images were obtained approximately at 25–30 seconds, 60 seconds, 3 minutes, and 20 minutes after contrast injection; the arterial phase timing was determined using a magnetic resonance fluoroscopic bolus detection technique.

All CEUS examinations were performed by faculty-level abdominal radiologists with at least 10 years of clinical experience with CEUS. CEUS was performed with a 1–5 or 1–7 MHz convex probe using LOGIQ E9 (GE Healthcare, Milwaukee, WI, USA) or RS80A (Samsung Medison, Seoul, Korea) ultrasound systems. Ultrasound-MRI fusion was routinely performed by using Volume Navigation (GE Healthcare) or S-fusion (Samsung Medison) for accurate lesion localization, regardless of the conspicuity of the lesion on gray-scale ultrasonography. The MRI sequence that most clearly visualized each lesion and adjacent anatomic landmarks was selected for image fusion. After image fusion, CEUS was performed, with MRI being displayed side-by-side. Contrast harmonic imaging was used with a default mechanical index setting of 0.20 to 0.26. The beam focus was located at the posterior margin of the liver. A perfluorobutane microbubble agent (Sonazoid, GE Healthcare, Oslo, Norway) was administered at a dose of 0.015 mL/kg body weight by manual bolus injection via a peripheral venous line, followed by a 10 mL saline flush. Arterial phase, portal venous phase, late vascular phase, and postvascular phase (i.e., Kupffer phase) images were obtained approximately at 10–40 seconds, 60–90 seconds, 3–4 minutes, and 10 minutes after contrast injection, in agreement with the Asian Federation of Societies for Ultrasound in Medicine and Biology recommendations [24].

Image Analysis

A board-certified radiologist (Y.Y.K., with 6 years of experience in liver imaging) retrospectively evaluated the presence of major and ancillary features of the hepatic observations on MRI, including APHE (MR-APHE), washout, TP hypointensity, HBP hypointensity, mild to moderate T2 hyperintensity, and restricted diffusion, and assigned LI-RADS categories based on LI-RADS version 2018 [1]. In addition, the following CEUS features were retrospectively and independently evaluated by two board-certified radiologists (J.A.H. and J.H.M., with 9 and 11 years of experience in liver imaging, respectively): (1) APHE on CEUS (i.e., CEUS-APHE), defined as hyperenhancement in the arterial phase that is neither rim-like nor peripheral discontinuous globular enhancement, and (2) a KPD, defined as no enhancement or marked hypoenhancement to the liver in the Kupffer phase [24]. KPD was examined instead of CEUS washout because the current LI-RADS does not address the use of Sonazoid for CEUS, and the APASL guidelines recommend the use of KPD on second-line CEUS [6,7]. For observations with a nodule-in-nodule appearance, CEUS features of the inner nodule were recorded. Discrepancies between the two readers were resolved by another board-certified radiologist (W.K.J., with 20 years of experience in liver imaging), and the consensus reading results were used for data analysis. The radiologists were aware of the study purpose but were blinded to patients' clinical information during image analysis. All images were reviewed using a picture archiving and communication system (Centricity Radiology RA 1000, GE Healthcare, Chicago, IL, USA).

Reference Standard

Electronic medical records and follow-up CT and/or MRI were reviewed to collect the reference standards. Observations were considered HCC if the lesion was pathologically diagnosed as HCC, or if compact Lipiodol uptake within the lesion was observed after transarterial chemoembolization [15,25,26]. Observations were considered benign if the lesion was pathologically diagnosed as benignancy, if the lesion resolved or was downgraded to LR-2 during follow-up, or if it remained stable for more than 24 months [27].

Statistical Analysis

Continuous variables were compared using the Student t-test or the Mann-Whitney U test, and categorical variables were compared using the chi-square test or the Fisher exact test according to the normality of the data distribution. Logistic regression analysis was performed to identify significant imaging features associated with HCC diagnosis. The backward elimination method was used to select variables for the multivariable analysis. Sensitivity, specificity, and accuracy for HCC were calculated for individual significant imaging features and their combinations, and comparisons were performed using the McNemar test. Subgroup analysis according to the LI-RADS category was performed. A two-sided P-value of less than 0.05 indicated statistical significance. The R package (version 3.6.1, The R Foundation for Statistical Computing, Vienna, Austria) was used for the analyses.

Results

Patient Characteristics

Of 543 potentially eligible patients, 350 patients met the inclusion criteria (Fig. 1). Of these, 20 patients who had CEUS or MRI of inadequate image quality, 169 patients who underwent subsequent treatment of index lesions with ablation therapy or radiotherapy, nine patients who were lost to follow-up after CEUS, and 48 patients who lacked a reference standard for the index lesion were excluded. Finally, 104 patients with 104 LR-3 or LR-4 observations were included.

The clinical characteristics of 104 patients (mean age, 59±8 years [range, 34 to 78 years]; 87 men) are shown in Table 1. Eighty-nine patients (85.6%) had hepatitis B virus infections, and 63 patients (60.6%) had liver cirrhosis. Sixty-one patients (58.7%) had a prior history of HCC. Patients with HCC (n=63) more commonly had a history of HCC than those with benign lesions (n=41) (71.4% vs. 39.0%, P=0.002). Serum α-fetoprotein level was significantly higher in patients with HCC than those with benign lesions (median, 10.0 vs. 3.5 ng/mL, P=0.008), but the proportion of patients with the level ≥20 ng/mL was comparable (33.3% vs. 24.4%, P=0.450). The median time interval between MRI and CEUS was 13 days (interquartile range, 9 to 19 days).

Imaging Features According to Diagnosis

Sixty-three observations were diagnosed as HCC by pathologic proof (n=12; interval between MRI and reference standard, 0.3–5.9 months), or compact Lipiodol uptake after transarterial chemoembolization (n=51; 0.3–6.0 months). Forty-one observations were diagnosed as benignancy by pathologic proof (n=7; high-grade dysplastic nodule [n=1], low grade dysplastic nodule [n=1], regenerative nodule [n=1], focal nodular hyperplasia [n=2], and hemangioma [n=2]), or follow-up imaging (n=34).

Washout (31.8% vs. 9.8%, P=0.018), TP hypointensity (81.0% vs. 26.8%, P<0.001), HBP hypointensity (87.3% vs. 51.2%, P<0.001), mild to moderate T2 hyperintensity (73.0% vs. 41.5%, P=0.003), restricted diffusion (85.7% vs. 43.9%, P<0.001), CEUS-APHE (69.8% vs. 43.9%, P=0.015), and KPD (77.8% vs. 22.0%, P<0.001) were more common in HCCs than in benign lesions (Table 2). The presence of both CEUS-APHE and KPD was more frequent in HCCs, and the absence of both CEUS-APHE and KPD was more common in benign lesions (Fig. 2).

Table 1. Patient characteristics

Variable	Total (n=104)	HCC (n=63)	Benign lesion (n=41)	P-value
Age (year)	59±8	60±7	57±9	0.052
Male sex	87 (83.7)	51 (81.0)	36 (87.8)	0.514
Etiology of liver disease				
HBV	88 (84.6)	54 (85.7)	34 (82.9)	0.895
HCV	5 (4.8)	3 (4.8)	2 (4.9)	
HBV and HCV	1 (1.0)	1 (1.6)	0	
Others	10 (9.6)	5 (7.9)	5 (12.2)	
Liver cirrhosis	63 (60.6)	39 (61.9)	24 (58.5)	0.890
Previous history of HCC	61 (58.7)	45 (71.4)	16 (39.0)	0.002
Serum AFP (ng/mL)	6.1 (2.7–21.1)	10.0 (3.9–24.3)	3.5 (2.4–10.9)	0.008
Serum AFP ≥20 ng/mL	31 (29.8)	21 (33.3)	10 (24.4)	0.450

Values are presented as mean±SD, number (%), or median (IQR).
HCC, hepatocellular carcinoma; HBV, hepatitis B virus; HCV, hepatitis C virus; AFP, α-fetoprotein; SD, standard deviation; IQR, interquartile range.

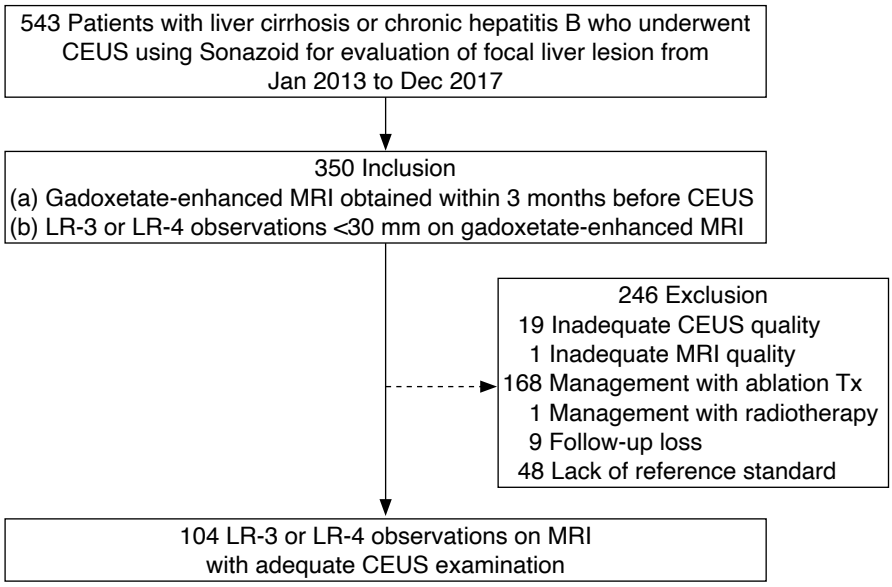

Fig. 1. Flow diagram of the study. CEUS, contrast-enhanced ultrasonography; LR-3, Liver Imaging Reporting and Data System category 3; LR-4, Liver Imaging Reporting and Data System category 4; MRI, magnetic resonance imaging; Tx, treatment.

There were 61 (58.7%) LR-3 and 43 (41.3%) LR-4 observations (Table 2). The frequency of MR-APHE and CEUS-APHE were comparable in both LR-3 HCC (61.5% vs. 57.7%) and LR-4 HCC (81.1% vs. 78.4%), although three (11.5%) LR-3 HCCs, and five (13.5%) LR-4 HCCs showed APHE only on CEUS. However, eight (30.8%) LR-3 HCCs, and 23 (62.2%) LR-4 HCCs showed KPD in the absence of washout on MRI. In LR-3 subgroup, TP hypointensity was significantly less frequent in benign lesions (22.9% vs. 76.9%, P<0.001). In both LR-3 and LR-4 subgroups, restricted diffusion was more common in HCCs (LR-3, 80.8% vs. 42.9%, P=0.007; LR-4, 89.2% vs. 50.0%, P=0.045). In the LR-4 subgroup, KPD was significantly more frequent in HCC (97.3% vs. 16.7%, P<0.001), and the presence of both CEUS-APHE and KPD was only observed in HCCs (78.4% of LR-4 HCCs). The presence of both CEUS-APHE and KPD on second-line CEUS enabled the additional detection of 40 HCCs (42.3% [n=11] of LR-3 HCCs and 78.4% [n=29] of LR-4 HCCs) in LR-3 or LR-4 observations on MRI. Only three benign lesions showed CEUS-APHE and KPD in the LR-3 subgroup.

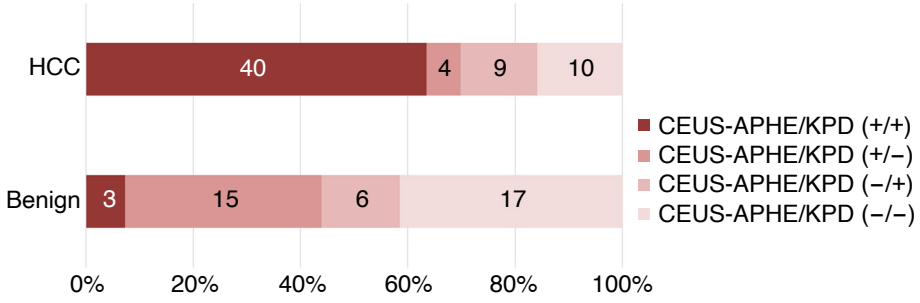

Fig. 2. Second-line CEUS features according to the diagnosis. APHE, arterial phase hyperenhancement; CEUS, contrast-enhanced ultrasonography; HCC, hepatocellular carcinoma; KPD, Kupffer phase defect.

Table 2. MRI and CEUS features according to the LI-RADS category

	Total (n=104)			LR-3 (n=61)			LR-4 (n=43)		
	HCC (n=63)	Benign lesion (n=41)	P-value	HCC (n=26)	Benign lesion (n=35)	P-value	HCC (n=37)	Benign lesion (n=6)	P-value
MRI features									
Size			0.058			0.226			>0.999
<10 mm	31 (49.2)	12 (29.3)		11 (42.3)	9 (25.7)		20 (54.1)	3 (50.0)	
10–19 mm	26 (41.3)	27 (65.9)		12 (46.2)	24 (68.6)		14 (37.8)	3 (50.0)	
≥20 mm	6 (9.5)	2 (4.9)		3 (11.5)	2 (5.7)		3 (8.1)	0	
MR-APHE	46 (73.0)	32 (78.1)	0.728	16 (61.5)	26 (74.3)	0.433	30 (81.1)	6 (100.0)	0.567
Washout	20 (31.8)	4 (9.8)	0.018	6 (23.1)	3 (8.6)	0.152	14 (37.8)	1 (16.7)	0.403
TP hypointensity	51 (81.0)	11 (26.8)	<0.001	20 (76.9)	8 (22.9)	<0.001	31 (83.8)	3 (50.0)	0.095
HBP hypointensity	55 (87.3)	21 (51.2)	<0.001	19 (73.1)	16 (45.7)	0.061	36 (97.3)	5 (83.3)	0.263
Mild to moderate T2 hyperintensity	46 (73.0)	17 (41.5)	0.003	17 (65.4)	14 (40.0)	0.089	29 (78.4)	3 (50.0)	0.164
Restricted diffusion	54 (85.7)	18 (43.9)	<0.001	21 (80.8)	15 (42.9)	0.007	33 (89.2)	3 (50.0)	0.045
CEUS features									
CEUS-APHE	44 (69.8)	18 (43.9)	0.015	15 (57.7)	15 (42.9)	0.375	29 (78.4)	3 (50.0)	0.164
KPD	49 (77.8)	9 (22.0)	<0.001	13 (50.0)	8 (22.9)	0.053	36 (97.3)	1 (16.7)	<0.001
CEUS enhancement pattern									
CEUS-APHE/KPD			<0.001			0.018			<0.001
(+)/(+)	40 (63.5)	3 (7.3)		11 (42.3)	3 (8.6)		29 (78.4)	0	
(+)/(–)	4 (6.5)	15 (36.6)		4 (15.4)	12 (34.3)		0	3 (50.0)	
(–)/(+)	9 (14.3)	6 (14.6)		2 (7.7)	5 (14.3)		7 (18.9)	1 (16.7)	
(–)/(–)	10 (15.9)	17 (41.5)		9 (34.6)	15 (42.9)		1 (2.7)	2 (33.3)	

Values indicate the number of lesions with percentages in parentheses.

MRI, magnetic resonance imaging; CEUS, contrast-enhanced ultrasonography; LI-RADS, Liver Imaging Reporting and Data System; HCC, hepatocellular carcinoma; LR-3, Liver Imaging Reporting and Data System category 3; LR-4, Liver Imaging Reporting and Data System category 4; APHE, arterial phase hyperenhancement; TP, transitional phase; HBP, hepatobiliary phase; KPD, Kupffer phase defect.

Logistic Regression Analysis

Multivariable analysis revealed that TP hypointensity (adjusted odds ratio [OR], 10.59; 95% confidence interval [CI], 2.96 to 37.89; P<0.001), restricted diffusion (adjusted OR, 7.55; 95% CI, 1.88 to 30.34; P=0.004), and KPD (adjusted OR, 7.16; 95% CI, 1.95 to 26.29; P=0.003) were independently associated with HCC diagnosis (Table 3). The adjusted OR for CEUS-APHE was 2.22 (95% CI, 0.67 to 7.39; P=0.194). Therefore, TP hypointensity, restricted diffusion, and KPD were identified as significant imaging features.

Performance of Significant Imaging Features for HCC Diagnosis

In all lesions, TP hypointensity (sensitivity and specificity, 81.0% and 73.2%, respectively) and KPD (sensitivity and specificity, 77.8% and 78.1%, respectively) showed the highest accuracy (77.9%) for HCC diagnosis among the significant imaging features (Table 4). The presence of at least two significant imaging features was optimal for HCC diagnosis (sensitivity, specificity, and accuracy of 88.9%, 78.1%, and 84.6%, respectively), with a significantly higher sensitivity than the presence of both CEUS-APHE and KPD (sensitivity, specificity, and accuracy of 63.5% [P=0.001], 92.7% [P=0.077], and 75.0% [P=0.089], respectively) (Fig. 3).

In the LR-3 subgroup, TP hypointensity had the highest accuracy (77.1%) with sensitivity and specificity of 76.9% and 77.1%, respectively (Fig. 4). In the LR-4 subgroup, KPD had the highest accuracy (95.4%), with sensitivity and specificity of 97.3% and 83.3%, respectively. The performance measures of the optimal criteria (the presence of at least two significant imaging features) were comparable to those of TP hypointensity in the LR-3 subgroup, and to those of KPD in the LR-4 subgroup (all P-values >0.999).

Discussion

In this study, the value of second-line CEUS with Sonazoid for the diagnosis of HCC was retrospectively analyzed in LR-3 and LR-4 observations on gadoxetate-enhanced MRI. It is notable that the presence of both CEUS-APHE and KPD on second-line CEUS enabled the additional detection of 63.5% of HCCs in this study. The sensitivity for HCC was 42.3% in the LR-3 subgroup and 78.4% in the LR-4 subgroup, with high specificity (91.4% in the LR-3 subgroup and 100.0% in the LR-4 subgroup). Furthermore, the combined use of second-line CEUS features and gadoxetate-enhanced MRI features showed the optimal diagnostic performance for HCC by improving the sensitivity for HCC to 88.9%. The presence of at least two significant imaging features (TP hypointensity, restricted diffusion, and KPD) showed a sensitivity of 76.9% in the LR-3 subgroup and 97.3% in the LR-4 subgroup. Although second-line CEUS showed additional diagnostic value in LR-3 and LR-4 observations with high specificity, the combined interpretation of MRI and CEUS enabled the better detection of HCC in these lesions.

The results of the present study suggest that second-line Sonazoid CEUS could be a viable alternative diagnostic imaging option in LR-3 and LR-4 observations [2,5]. The APASL guidelines highly recommend that second-line CEUS with Sonazoid should be used

Table 3. Imaging features associated with HCC diagnosis

Variable	Univariable analysis		Multivariable analysis	
	OR (95% CI)	P-value	OR (95% CI)	P-value
Size (mm) (reference: <10)				
10–19	0.37 (0.16–0.88)	0.024	2.26 (0.55–9.27)	0.259
≥20	1.16 (0.21–6.57)	0.866	12.52 (0.95–164.11)	0.054
LR-4 (reference: LR-3)	8.30 (3.05–22.58)	<0.001	2.88 (0.75–11.08)	0.124
MR-APHE	0.76 (0.30–1.92)	0.563		
Washout	4.30 (1.35–13.72)	0.014		
TP hypointensity	11.59 (4.55–29.50)	<0.001	10.59 (2.96–37.89)	<0.001
HBP hypointensity	6.55 (2.50–17.13)	<0.001		
Mild to moderate T2 hyperintensity	3.82 (1.66–8.80)	0.002		
Restricted diffusion	7.67 (3.00–19.57)	<0.001	7.55 (1.88–30.34)	0.004
CEUS-APHE	2.96 (1.31–6.71)	0.009	2.22 (0.67–7.39)	0.194
KPD	12.44 (4.82–32.13)	<0.001	7.16 (1.95–26.29)	0.003

Variable selection was performed using the backward elimination method, and CEUS-APHE was fixed during variable selection.

HCC, hepatocellular carcinoma; OR, odds ratio; CI, confidence interval; LR-4, Liver Imaging Reporting and Data System category 4; LR-3, Liver Imaging Reporting and Data System category 3; APHE, arterial phase hyperenhancement; TP, transitional phase; HBP, hepatobiliary phase; CEUS, contrast-enhanced ultrasonography; KPD, Kupffer phase defect.

Table 4. Diagnostic performance of significant imaging features for HCC diagnosis

LI-RADS category	Performance measure (%) (95% CI)		
	Sensitivity	Specificity	Accuracy
All			
Individual imaging features			
TP hypointensity	81.0 (69.1–89.8)	73.2 (57.1–85.8)	77.9 (68.7–85.4)
Restricted diffusion	85.7 (74.6–93.3)	56.1 (39.8–71.5)	74.0 (64.5–82.1)
KPD	77.8 (65.5–87.3)	78.1 (62.4–89.4)	77.9 (68.7–85.4)
Combination of imaging features			
At least one	98.4 (91.5–100.0)	34.2 (20.1–50.6)	73.1 (63.5–81.3)
At least two	88.9 (78.4–95.4)	78.1 (62.4–89.4)	84.6 (76.2–90.9)
All three	57.1 (44.1–69.5)	95.1 (83.5–99.4)	72.1 (62.5–80.5)
CEUS-APHE and KPD	63.5 (50.4–75.3)	92.7 (80.1–98.5)	75.0 (65.6–83.0)
LR-3			
Individual imaging features			
TP hypointensity	76.9 (56.4–91.0)	77.1 (59.9–89.6)	77.1 (64.5–86.9)
Restricted diffusion	80.8 (60.7–93.5)	57.1 (39.4–73.7)	67.2 (54.0–78.7)
KPD	50.0 (29.9–70.1)	77.1 (59.9–89.6)	65.6 (52.3–77.3)
Combination of imaging features			
At least one	96.2 (80.4–99.9)	40.0 (23.9–57.9)	63.9 (50.6–75.8)
At least two	76.9 (56.4–91.0)	77.1 (59.9–89.6)	77.1 (64.5–86.9)
All three	34.6 (17.2–55.7)	94.3 (80.8–99.3)	68.9 (55.7–80.1)
CEUS-APHE and KPD	42.3 (23.4–63.1)	91.4 (76.9–98.2)	70.5 (57.4–81.5)
LR-4			
Individual imaging features			
TP hypointensity	83.8 (68.0–93.8)	50.0 (11.8–88.2)	79.1 (64.0–90.0)
Restricted diffusion	89.2 (74.6–97.0)	50.0 (11.8–88.2)	83.7 (69.3–93.2)
KPD	97.3 (85.8–99.9)	83.3 (35.9–99.6)	95.4 (84.2–99.4)
Combination of imaging features			
At least one	73.0 (55.9–86.2)	100.0 (54.1–100.0)	76.7 (61.4–88.2)
At least two	97.3 (85.8–99.9)	83.3 (35.9–99.6)	95.4 (84.2–99.4)
All three	73.0 (55.9–86.2)	100.0 (54.1–100.0)	76.7 (61.4–88.2)
CEUS-APHE and KPD	78.4 (61.8–90.2)	100.0 (54.1–100.0)	81.4 (66.6–91.6)

HCC, hepatocellular carcinoma; LI-RADS, Liver Imaging Reporting and Data System; CI, confidence interval; TP, transitional phase; KPD, Kupffer phase defect; CEUS, contrast-enhanced ultrasonography; APHE, arterial phase hyperenhancement.

to diagnose HCC in observations that do not show MR-APHE but depict HBP hypointensity on gadoxetate-enhanced MRI [6]. This study expanded the APASL indication to LR-3 or LR-4 observations, and showed a promising diagnostic performance for HCC. Of note, lack of washout on gadoxetate-enhanced MRI was one of the major reasons for HCC to be categorized as LR-3 or LR-4 on MRI. In the LR-4 subgroup, KPD provided a diagnosis that was both highly sensitive and highly specific, and the presence of both CEUS-APHE and KPD was only observed in HCC in the LR-4 subgroup. Prior studies have suggested that KPD is more specific to progressed HCC than HBP hypointensity [10,12,16]. According to another study [13], Kupffer phase iso-enhancement, especially when CEUS-APHE is absent, rarely indicated HCC, which is in agreement with the present study results. Considering that KPD showed comparable diagnostic performance to the optimal criteria in the LR-4 subgroup, a second-line diagnostic workup using Sonazoid CEUS can be especially necessary for LR-4 observations.

However, the incremental value of CEUS-APHE was somewhat smaller than expected. A recent study using a purely intravascular CEUS agent showed a comparable frequency of CEUS-APHE

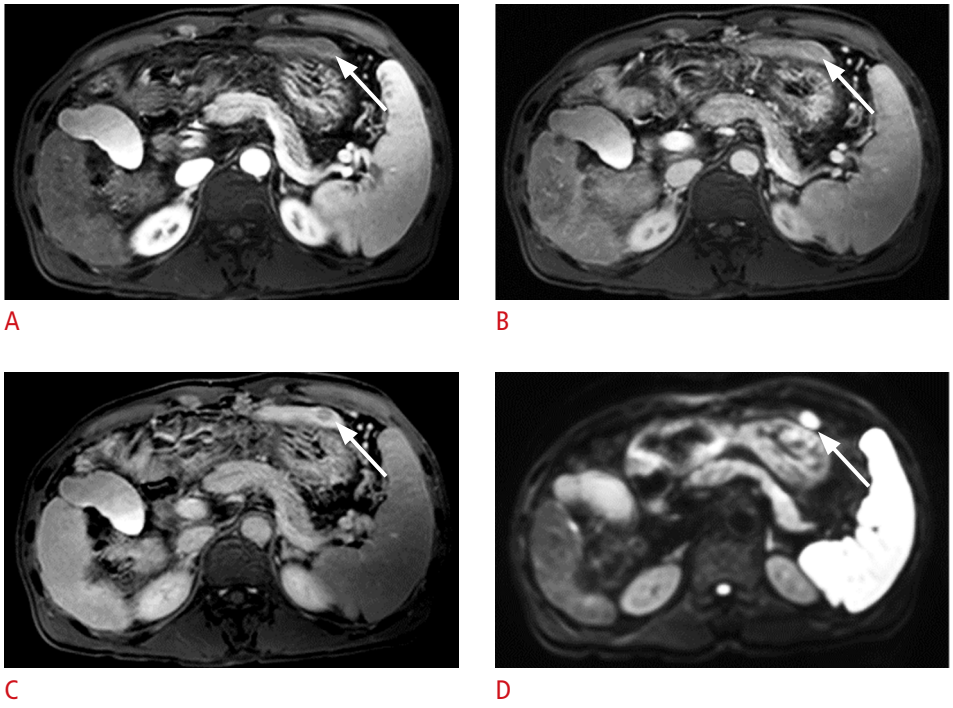

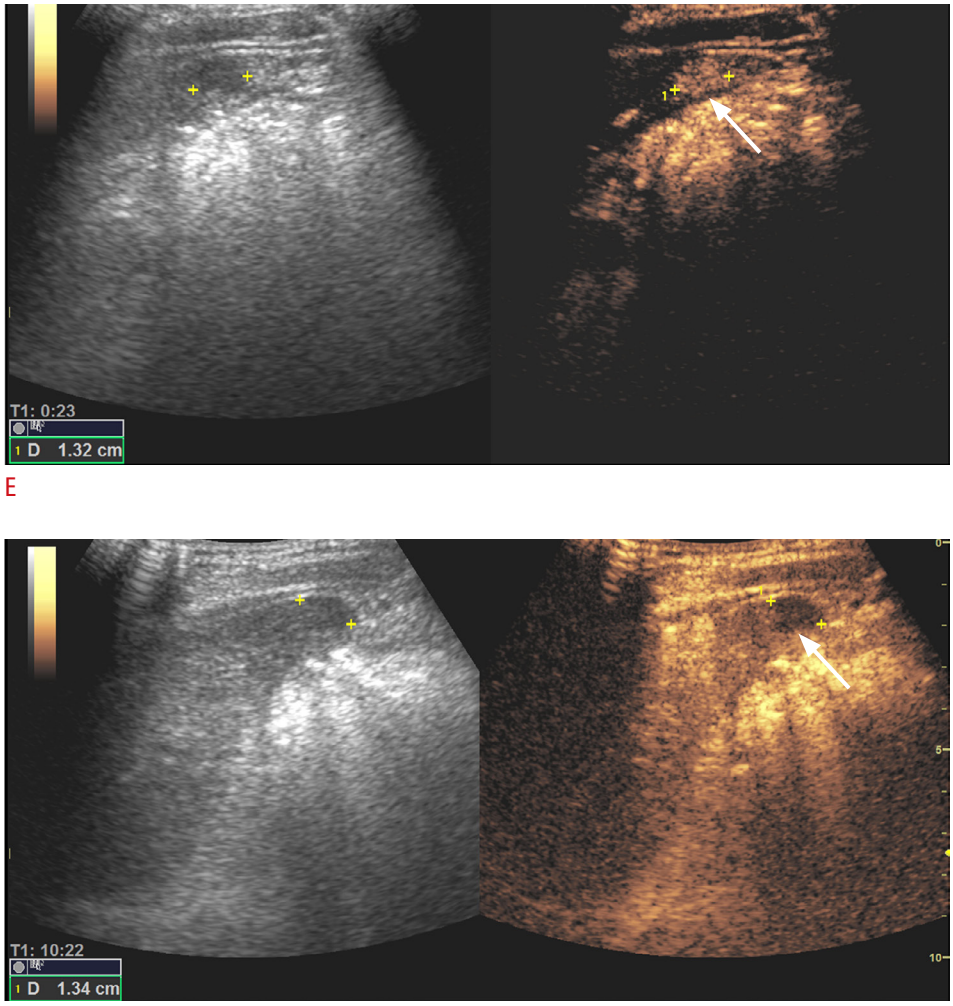

Fig. 3. An 11-mm LR-4 observation in a 56-year-old man with hepatitis B virus–related liver cirrhosis and a prior history of HCC, which showed all significant imaging features and was pathologically diagnosed as HCC.
A, B. On gadoxetate-enhanced magnetic resonance imaging, the observation (arrow) shows no clear APHE (MR-APHE) (A) or washout (B). C, D. The observation (arrow) shows transitional phase hypointensity (C), hepatobiliary phase hypointensity (not shown), mild to moderate T2 hyperintensity (not shown), and restricted diffusion on b=800 s/mm^2 image (D). E, F. On second-line CEUS performed 24 days later, CEUS-APHE (E) and Kupffer phase defect (arrow) are demonstrated (F). LR-4, Liver Imaging Reporting and Data System category 4; HCC, hepatocellular carcinoma; APHE, arterial phase hyperenhancement; CEUS, contrast-enhanced ultrasonography.

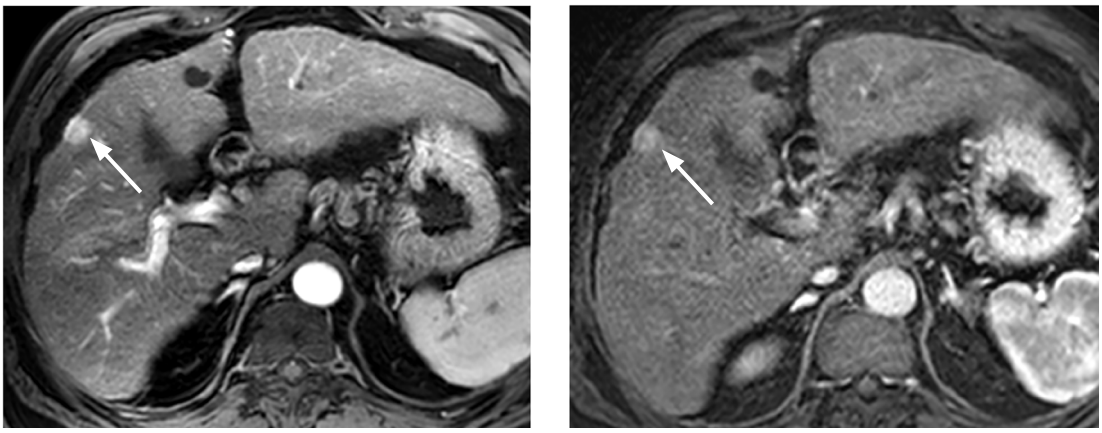

A D

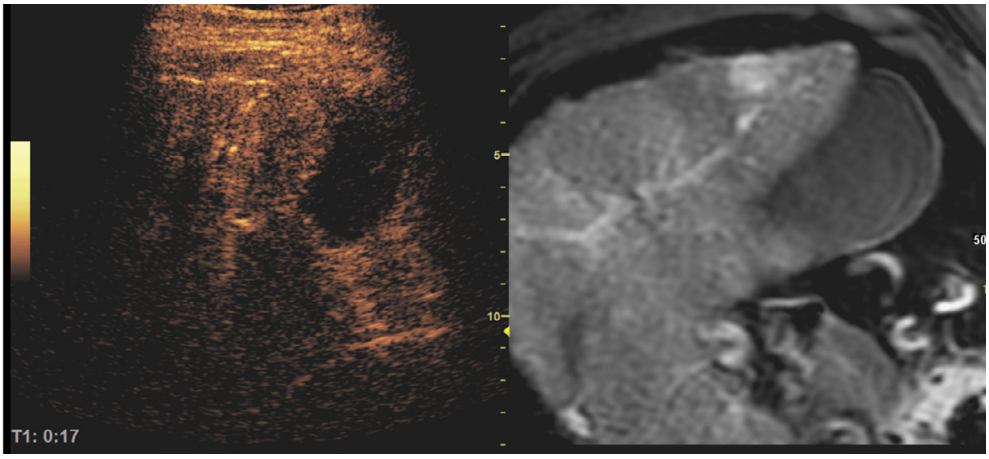

B

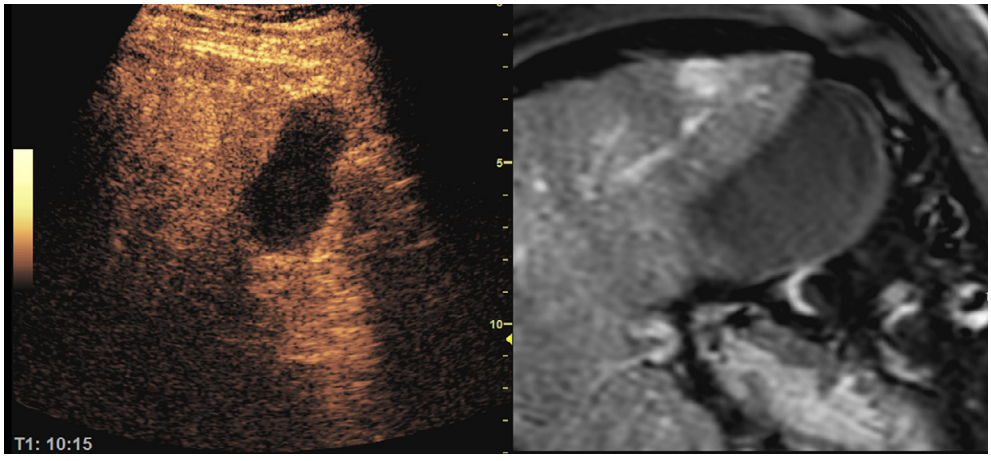

C

Fig. 4. A 15-mm LR-3 observation in a 65-year-old man with liver cirrhosis of unknown etiology and a prior history of hepatocellular carcinoma, which showed no significant imaging features and was finally determined to be benign.

A. On the index gadoxetate-enhanced MRI, the observation (arrow) shows arterial phase hyperenhancement but no washout or ancillary features favoring malignancy (not shown). B, C. On contrast-enhanced ultrasonography using Sonazoid performed 11 days later, the observation is isoechoic to the liver in the arterial phase (B) and the Kupffer phase (C). D. On gadoxetate-enhanced MRI taken 25 months after the index MRI, the observation (arrow) remains unchanged in size and characteristics. LR-3, Liver Imaging Reporting and Data System category 3; MRI, magnetic resonance imaging.

and MR-APHE (77.7% vs. 72.8%) in LR-3, LR-4, LR-5, and LR-M observations [28]. In this study using Sonazoid, approximately 10% of HCCs showed APHE only on CEUS, not on MRI. Although CEUS may display APHE in some cases in which gadoxetate-enhanced MRI fails to capture APHE [29], the added value of CEUS-APHE may not be substantial, as shown by the results of multivariable logistic regression analysis in the present study. Nonetheless, CEUS-APHE was significantly less frequent in benign lesions than in HCCs (43.9% vs. 69.8%), suggesting that it may be more specific than MR-APHE benign lesion vs. HCC (78.1% vs. 73.0%).

The combined interpretation of gadoxetate-enhanced MRI and second-line CEUS was optimal rather than using CEUS features alone. Interestingly, ancillary features favoring malignancy in the LI-RADS diagnostic algorithm, such as TP hypointensity and restricted diffusion, were designated as significant imaging features. TP hypointensity may help overcome the limitation of portal venous phase washout on gadoxetate-enhanced MRI [19]. In addition, restricted diffusion is regarded as an indicator of progressed HCC in comparison with early HCC or dysplastic nodules [30,31]. These features have also been emphasized as key ancillary features of LI-RADS [4,32,33]. The optimal diagnostic criteria identified herein may be a useful strategy for applying ancillary MRI features to LR-3 and LR-4 observations.

This study has some limitations. First, selection bias may have been introduced by retrospectively analyzing observations that were evaluated both with MRI and CEUS. Further studies with a prospective study design are warranted to overcome this limitation and strengthen the results. Second, the diagnostic value of portal venous phase or late vascular phase CEUS images was not evaluated, but warrants further investigation. Third, inter-operator variability in CEUS examinations may have existed. However, the variability would be small, as ultrasound-MRI fusion was routinely performed to enable accurate localization of observations noted on MRI. Fourth, the majority (85.6%) of patients had hepatitis B virus infection, which may limit the generalizability of the results.

In conclusion, second-line CEUS with Sonazoid can additionally detect HCC in LR-3 or LR-4 observations on gadoxetate-enhanced MRI with excellent specificity. Combined interpretation of MRI and CEUS, with a focus on TP hypointensity, restricted diffusion, and KPD, may be an optimal strategy for further characterizing LR-3 and LR-4 observations on gadoxetate-enhanced MRI.

ORCID: Yeun-Yoon Kim: https://orcid.org/0000-0003-2018-5332; Ji Hye Min: https://orcid.org/0000-0002-8496-6771; Jeong Ah Hwang: https://orcid.org/0000-0002-8012-995X; Woo Kyoung Jeong: https://orcid.org/0000-0002-0676-2116; Dong Hyun Sinn: https://orcid.org/0000-0002-7126-5554; Hyo Keun Lim: https://orcid.org/0000-0003-3269-7503

※Author affiliations

[1]Department of Radiology and Center for Imaging Sciences, Samsung Medical Center, Sungkyunkwan University School of Medicine, Seoul; [2]Department of Medicine, Samsung Medical Center, Sungkyunkwan University School of Medicine, Seoul, Korea

Author Contributions

Conceptualization: Min JH, Jeong WK, Shin DH, Lim HK. Data acquisition: Kim YY, Min JH, Hwang JA, Jeong WK. Data analysis or interpretation: Kim YY, Min JH, Hwang JA, Jeong WK, Shin DH, Lim HK. Drafting of the manuscript: Kim YY. Critical revision of the manuscript: Min JH, Hwang JA, Jeong WK, Shin DH, Lim HK. Approval of the final version of the manuscript: all authors.

Conflict of Interest

No potential conflict of interest relevant to this article was reported.

Supplementary Material

Supplementary Table 1. MRI parameters (https://doi.org/10.14366/usg.21198).

References

1. Chernyak V, Fowler KJ, Kamaya A, Kielar AZ, Elsayes KM, Bashir MR, et al. Liver Imaging Reporting and Data System (LI-RADS) Version 2018: imaging of hepatocellular carcinoma in at-risk patients. Radiology 2018;289:816-830.
2. Marrero JA, Kulik LM, Sirlin CB, Zhu AX, Finn RS, Abecassis MM, et al. Diagnosis, staging, and management of hepatocellular carcinoma: 2018 practice guidance by the American Association for the Study of Liver Diseases. Hepatology 2018;68:723-750.
3. Lee S, Kim YY, Shin J, Hwang SH, Roh YH, Chung YE, et al. CT and MRI Liver Imaging Reporting and Data System version 2018 for hepatocellular carcinoma: a systematic review with meta-analysis. J Am Coll Radiol 2020;17:1199-1206.
4. Kim YY, Choi JY, Kim SU, Lee M, Park MS, Chung YE, et al. MRI ancillary features for LI-RADS category 3 and 4 observations: improved categorization to indicate the risk of hepatic malignancy. AJR Am J Roentgenol 2020;215:1354-1362.
5. Mitchell DG, Bashir MR, Sirlin CB. Management implications and outcomes of LI-RADS-2, -3, -4, and -M category observations. Abdom Radiol (NY) 2018;43:143-148.
6. Omata M, Cheng AL, Kokudo N, Kudo M, Lee JM, Jia J, et al. Asia-Pacific clinical practice guidelines on the management of hepatocellular carcinoma: a 2017 update. Hepatol Int 2017;11:317-370.
7. Quaia E. State of the art: LI-RADS for contrast-enhanced US. Radiology 2019;293:4-14.
8. Lee J, Jeong WK, Lim HK, Kim AY. Focal nodular hyperplasia of the liver: contrast-enhanced ultrasonographic features with sonazoid. J Ultrasound Med 2018;37:1473-1480.
9. Chung YE, Kim KW. Contrast-enhanced ultrasonography: advance and current status in abdominal imaging. Ultrasonography 2015;34:3-18.
10. Ohama H, Imai Y, Nakashima O, Kogita S, Takamura M, Hori M, et al. Images of Sonazoid-enhanced ultrasonography in multistep hepatocarcinogenesis: comparison with Gd-EOB-DTPA-enhanced MRI. J Gastroenterol 2014;49:1081-1093.

11. Maruyama H, Takahashi M, Ishibashi H, Yoshikawa M, Yokosuka O. Contrast-enhanced ultrasound for characterisation of hepatic lesions appearing non-hypervascular on CT in chronic liver diseases. Br J Radiol 2012;85:351-357.
12. Sugimoto K, Moriyasu F, Saito K, Taira J, Saguchi T, Yoshimura N, et al. Comparison of Kupffer-phase Sonazoid-enhanced sonography and hepatobiliary-phase gadoxetic acid-enhanced magnetic resonance imaging of hepatocellular carcinoma and correlation with histologic grading. J Ultrasound Med 2012;31:529-538.
13. Arita J, Takahashi M, Hata S, Shindoh J, Beck Y, Sugawara Y, et al. Usefulness of contrast-enhanced intraoperative ultrasound using Sonazoid in patients with hepatocellular carcinoma. Ann Surg 2011;254:992-999.
14. Hope TA, Fowler KJ, Sirlin CB, Costa EA, Yee J, Yeh BM, et al. Hepatobiliary agents and their role in LI-RADS. Abdom Imaging 2015;40:613-625.
15. Bae JS, Kim JH, Yu MH, Lee DH, Kim HC, Chung JW, et al. Diagnostic accuracy of gadoxetic acid-enhanced MR for small hypervascular hepatocellular carcinoma and the concordance rate of Liver Imaging Reporting and Data System (LI-RADS). PLoS One 2017;12:e0178495.
16. Arita J, Hasegawa K, Takahashi M, Hata S, Shindoh J, Sugawara Y, et al. Correlation between contrast-enhanced intraoperative ultrasound using Sonazoid and histologic grade of resected hepatocellular carcinoma. AJR Am J Roentgenol 2011;196:1314-1321.
17. Kudo M, Hatanaka K, Maekawa K. Sonazoid-enhanced ultrasound in the diagnosis and treatment of hepatic tumors. J Med Ultrasound 2008;16:130-139.
18. Kudo M. Defect reperfusion imaging with Sonazoid®: a breakthrough in hepatocellular carcinoma. Liver Cancer 2016;5:1-7.
19. Kim DH, Choi SH, Kim SY, Kim MJ, Lee SS, Byun JH. Gadoxetic acid-enhanced MRI of hepatocellular carcinoma: value of washout in transitional and hepatobiliary phases. Radiology 2019;291:651-657.
20. Lee S, Kim SS, Chang DR, Kim H, Kim MJ. Comparison of LI-RADS 2018 and KLCA-NCC 2018 for noninvasive diagnosis of hepatocellular carcinoma using magnetic resonance imaging. Clin Mol Hepatol 2020;26:340-351.
21. Byun J, Choi SH, Byun JH, Lee SJ, Kim SY, Won HJ, et al. Comparison of the diagnostic performance of imaging criteria for HCCs ≤3.0 cm on gadoxetate disodium-enhanced MRI. Hepatol Int 2020;14:534-543.
22. Jeon SK, Lee JM, Joo I, Yoo J, Park JY. Comparison of guidelines for diagnosis of hepatocellular carcinoma using gadoxetic acid-enhanced MRI in transplantation candidates. Eur Radiol 2020;30:4762-4771.
23. Hwang JA, Jeong WK, Min JH, Kim YY, Heo NH, Lim HK. Sonazoid-enhanced ultrasonography: comparison with CT/MRI Liver Imaging Reporting and Data System in patients with suspected hepatocellular carcinoma. Ultrasonography 2021;40:486-498.
24. Lee JY, Minami Y, Choi BI, Lee WJ, Chou YH, Jeong WK, et al. The AFSUMB consensus statements and recommendations for the clinical practice of contrast-enhanced ultrasound using Sonazoid. Ultrasonography 2020;39:191-220.
25. Miyayama S, Yamashiro M, Hashimoto M, Hashimoto N, Ikuno M, Okumura K, et al. Identification of small hepatocellular carcinoma and tumor-feeding branches with cone-beam CT guidance technology during transcatheter arterial chemoembolization. J Vasc Interv Radiol 2013;24:501-508.
26. Li JJ, Zheng JS, Cui SC, Cui XW, Hu CX, Fang D, et al. C-arm Lipiodol CT in transcatheter arterial chemoembolization for small hepatocellular carcinoma. World J Gastroenterol 2015;21:3035-3040.
27. Vernuccio F, Cannella R, Meyer M, Choudhoury KR, Gonzales F, Schwartz FR, et al. LI-RADS: diagnostic performance of hepatobiliary phase hypointensity and major imaging features of LR-3 and LR-4 lesions measuring 10–19 mm with arterial phase hyperenhancement. AJR Am J Roentgenol 2019;213:W57-W65.
28. Kang HJ, Lee JM, Yoon JH, Han JK. Role of contrast-enhanced ultrasound as a second-line diagnostic modality in noninvasive diagnostic algorithms for hepatocellular carcinoma. Korean J Radiol 2021;22:354-365.
29. Kang HJ, Kim JH, Joo I, Han JK. Additional value of contrast-enhanced ultrasound (CEUS) on arterial phase non-hyperenhancement observations (≥2 cm) of CT/MRI for high-risk patients: focusing on the CT/MRI LI-RADS categories LR-3 and LR-4. Abdom Radiol (NY) 2020;45:55-63.
30. Hwang J, Kim YK, Jeong WK, Choi D, Rhim H, Lee WJ. Nonhypervascular hypointense nodules at gadoxetic acid-enhanced MR imaging in chronic liver disease: diffusion-weighted Imaging for characterization. Radiology 2015;277:309.
31. Joo I, Kim SY, Kang TW, Kim YK, Park BJ, Lee YJ, et al. Radiologic-pathologic correlation of hepatobiliary phase hypointense nodules without arterial phase hyperenhancement at gadoxetic acid-enhanced MRI: a multicenter study. Radiology 2020;296:335-345.
32. Cannella R, Vernuccio F, Sagreiya H, Choudhury KR, Iranpour N, Marin D, et al. Liver Imaging Reporting and Data System (LI-RADS) v2018: diagnostic value of ancillary features favoring malignancy in hypervascular observations ≥ 10 mm at intermediate (LR-3) and high probability (LR-4) for hepatocellular carcinoma. Eur Radiol 2020;30:3770-3781.
33. Kang JH, Choi SH, Byun JH, Kim DH, Lee SJ, Kim SY, et al. Ancillary features in the Liver Imaging Reporting and Data System: how to improve diagnosis of hepatocellular carcinoma ≤ 3 cm on magnetic resonance imaging. Eur Radiol 2020;30:2881-2889.